High-performance electrical properties of La-based perovskite ceramics for the functional phase of thick film resistors

Yongcheng Lu (yongcheng1004@163.com)
University of Electronic Science and Technology of China https://orcid.org/0000-0003-1205-5642
Yuanxun Li
University of Electronic Science and Technology of China
Daming Chen
Hainan University
Rui Peng
University of Electronic Science and Technology of China
Qinghui Yang
University of Electronic Science and Technology of China
Shijun Zhang
Mianyang Beidou Electronics Co., Ltd

Research Article

Keywords: Thick film resistors, Functional phase, Resistivity, perovskite

Posted Date: December 10th, 2020

DOI: https://doi.org/10.21203/rs.3.rs-123794/v1

Version of Record: A version of this preprint was published at Journal of Alloys and Compounds on June 1st, 2021. See the published version at https://doi.org/10.1016/j.jallcom.2021.159035.

Abstract

In order to explore an economical functional phase alternative material for thick film resistors, the crystal structure, microstructure, and electrical properties of (1-x)LSCN + xLCNZ (x = 0.0–1.0) composite ceramics were studied through solid-state reaction experiments. The composite ceramics were characterized by x–ray diffraction, scanning electron microscopy, energy dispersive x–ray spectroscopy, and DC four–probe method. Results suggested that the main phases of LSCN and LCNZ were formed, along with a small part of impurity phases. The addition of LCNZ to LSCN decreased the electrical conductivity and changed the TCR from positive to negative. Zero TCR could be achieved around $0.6 < x < 0.8$ and relatively low absolute TCR values could be obtained for the samples of $0.4 \leq x \leq 0.8$. The ceramic of 0.6LSCN + 0.4LCNZ showed the optimal performances of conductivity = 1923 S/cm, TCR = 379.54 ppm/℃, and relative density = 95.05%.

1. Introduction

Thick film resistors (TFRs) are one kind of thick film component which has been applied extensively in hybrid circuits for power conversion, current limiting, voltage division, etc. [1–3]. TFRs can be formed by screen-printing the paste onto a substrate, followed by drying and firing in a belt furnace [4]. And the paste usually comprises functional phase, glass phase, and organic vehicle [5, 6]. Ag/PdO, RuO_2, IrO_2, $Bi_2Ru_2O_7$, and $Pb_2Ru_2O_{6.5}$ are typical functional phases of TFRs, which manifest high conductivity (for broad range of resistance value), positive TCR at temperatures of 25–125 ℃, long–term stability, and high–temperature stability [7–10]. However, all of them contains precious metal elements which is not beneficial to lower the production cost of manufacturing TFRs. Considering this problem, some base metals (like Cu, Al), SnO_2 and MoO_2, or carbon paste, have been researched as functional phase of TFRs [11–14]. Nevertheless, either their sintering processes depend on inert atmospheres or their electrical performances (resistance and TCR) are poor [3, 13]. Therefore, it still makes sense to study more economical functional phase alternative materials.

Perovskite oxides of $La_{1-x}Sr_xCoO_{3-\delta}$ and $LaCo_{1-x}Ni_xO_3$ have aroused wide concern in the field of solid oxide fuel cell cathodes, thermoelectric conversion, and oxygen–permeable membranes due to their unusual magnetic and electrical properties [15–20]. For $La_{1-x}Sr_xCoO_{3-\delta}$, as 50% Sr^{2+} substitutes to La^{3+} site, abundant hole carriers are introduced and almost the same amount of Co^{3+} ions would be converted to Co^{4+} in this system, which strengthens the double exchange interactions between Co^{3+} and Co^{4+} ions [21]. Furthermore, the ion-conversion optimizes the electron transport and provides this material with excellent conductivity [22]. For $LaCo_{1-x}Ni_xO_3$, researchers believed that the replacement of Ni for Co can improve the electron density and carrier concentration, as well as broaden the width of the itinerant conduction band, leading to a reduction in resistivity [23–26]. In our previous investigations, $La_{0.5}Sr_{0.5}Co_{0.96}Ni_{0.04}O_{3-\delta}$ (LSCN) shows the highest conductivity of 3155 S/cm and positive TCR value of 2295.4 ppm/℃ [25], and those of $LaCo_{0.4}Ni_{0.58}Zn_{0.02}O_3$ (LCNZ) are 970.9 S/cm and negative TCR value of -872.82 ppm/℃ [27]. Besides, these two materials are stable in air even at high temperatures. As

it is known that the TCR value of the TFRs is usually adjusted by altering the quantitative ratio between functional phase with positive TCR and glass phase with negative TCR [28]. If the TCR of the functional phase is close to zero, a new route to produce TFRs would be achieved without glass phase. Therefore, zero TCR might be realized by adding the LCNZ ceramic into the LSCN ceramic.

Thus, the present study was performed to study the crystal structure, microstructure, and electrical properties of (1-x)LSCN + xLCNZ (x = 0.0–1.0) composite ceramics, and to investigate the possibility to be an economical functional phase for TFRs.

2. Experimental

La_2O_3, $SrCO_3$, Co_2O_3, NiO, and ZnO (all of these powders were Analytical Reagent and were purchased from Chron Co. Ltd., Chengdu, China) were used to synthesize the composite ceramics via the conventional solid–state reaction. The powders were weighted in accordance with the stoichiometric ratio of LSCN and LCNZ ceramics and were ball-milled for 24 h separately. Subsequently, both of the milled mixtures were dried and calcined at 900 ℃ for 12 h. The resulting powders were mixed and ball-milled for 24 h again based on the x value of (1-x)LSCN + xLCNZ (x =0.0–1.0, molar ratio). The dried powders were ground thoroughly and shaped into disk by adding 5 wt% binder. Eventually, these disks were sintered at 1200 ℃ for 6 h in air.

The crystal structure of these composite ceramics was determined through x–ray diffraction (XRD: DX–2700, Haoyuan Co.) with Cu–K_α radiation. The structure refinement was performed using Fullprof software based on the XRD data. Scanning electron microscopy (SEM: JEOL, JSM–6490LV) and energy dispersive x–ray spectroscopy (EDS) were adopted to observed the microstructure and element distribution. The bulk density was obtained through Archimedes method, and relative density was calculated by Eq. (1),

$$\rho = \frac{W_1 - W_2}{W_1/\rho_1 + W_2/\rho_2} \quad (1)$$

where W_1 and W_2 denote the weight fraction of two materials; ρ_1 and ρ_2 are the corresponding theoretical density [29]. The electrical resistivities were examined using the DC four–probe (RST–9) method within the range of 25–125 °C. The TCR value could be obtained by Eq. (2),

$$TCR = \frac{\rho_{125} - \rho_{25}}{\rho_{25}(T - T_0)} \times 10^6 \ (\mathrm{ppm/℃}) \quad (2)$$

where ρ_{25} and ρ_{125} mean the resistivity at 25 °C (T_0) and 125 °C (T), respectively.

3. Results And Discussion

Figure 1(a–b) presents the XRD patterns of (1-x)LSCN + xLCNZ (x = 0.0–1.0) composite ceramics. The phases of $La_{0.5}Sr_{0.5}CoO_{2.91}$ (JCPDS#48–0122) and $LaCo_{0.4}Ni_{0.6}O_3$ (JCPDS#32–0296) were formed in the samples of x = 0.0 and x = 1.0, respectively. And the main phases of other composite ceramics can be indexed to the combination of these two standard patterns. As the x value increases, the diffraction peak intensity of $LaCo_{0.4}Ni_{0.6}O_3$ strengthens. This variation can be noted at the peaks of (110) and (104). However, the overall peak intensity of the composite ceramics weakens monotonously with the increase of x except for the specimen of x = 1.0. Moreover, the impurity phase of NiO emerges as $x \geq 0.2$, while the phase of $La_{1.2}Sr_{0.8}NiO_4$ becomes apparent in the range of $x \geq 0.4$. The XRD refinements were performed based on the Rietveld method. The refinement pattern and detail fitting parameters are showed in Fig. 1c and Table I. The profile of refinement matches well with the experiment data, and the fitting parameters are acceptable. The calculated fraction and designed fraction values of each phase are displayed in Fig. 2. The calculated fraction of LSCN and LCNZ deviates slightly from the designed value due to the presence of impurity phases.

Table I. The lattice and fitting parameters of (1-x)LSCN + xLCNZ (x = 0.0–1.0) composite ceramics acquired from refinement.

Parameter	x = 0.0	x = 0.2	x = 0.4	x = 0.6	x = 0.8	x = 1.0
LSCN						
a (Å)	5.4290	5.4363	5.4421	5.4249	5.4398	\
b (Å)	5.4290	5.4363	5.4421	5.4249	5.4398	\
c (Å)	13.2527	13.2352	13.2159	13.2264	13.2457	\
Vol ($Å^3$)	338.279	338.744	338.974	337.096	339.449	\
LCNZ						
a (Å)	\	5.4366	5.4424	5.4520	5.4582	5.4615
b (Å)	\	5.4366	5.4424	5.4520	5.4582	5.4615
c (Å)	\	13.2365	13.2052	13.1726	13.1463	13.1318
Vol ($Å^3$)	\	338.811	338.729	339.084	339.176	339.216
R_p (%)	13.6	10.9	11.8	15.2	13.8	9.56
R_{wp} (%)	8.34	6.46	7.52	9.71	10.2	7.32
R_{exp} (%)	10.11	3.36	4.44	4.43	4.01	3.12
χ^2	0.681	3.69	2.87	4.79	6.48	5.50

The microstructure of (1-x)LSCN + xLCNZ (x = 0.2–0.8) composite ceramics was examined by SEM and is displayed in Fig. 4(a–d). Closely compact microstructures can be seen in these samples except the specimen of x = 0.8. For the composite ceramic of x = 0.2, large grains account for the majority, along with some unobvious small grains and trapped pores. With further addition of LCNZ, the average grain size decreases and small grains grow in the samples of x = 0.4 and x = 0.6 (Figs. 4b and 4c), which might due to the insufficient energy required for grain boundaries migration and/or the migration was blocked by impurity phases during sintering [34]. As the LCNZ content reaches 0.8, visible pores and strip-like grains emerge. The variation of microstructures confirms the outcome of relative density. The EDS mapping images of 0.6LSCN + 0.4LCNZ ceramic are exhibited Fig. 4(e–k), which manifest that the phases of LSCN and LCNZ are almost homogeneously distributed in the composite ceramic. Nevertheless, the element distribution of La, Sr, and Ni is not as uniform as that of Co, Zn, and O. In detail, there are some La-lacking, Sr-rich, and Ni-rich regions in this range; and the region lacking La basically corresponds to the region rich in Sr. These uneven regions could be the existence of impurity phases of $La_{1.2}Sr_{0.8}NiO_4$ and NiO. Figure 5 shows the elemental composition of composite ceramics of x = 0.4 and x = 0.6 detected by EDS point scan. Results demonstrate that the basic elements can be detected in these materials. For these two specimens, the element ratio at spot-1 is essentially consistent with the designed value, while the element of spot-2 is rich in Sr. These outcomes are in accordance with the phenomena of EDS mapping. Moreover, the results also testify the observations displayed in XRD.

4. Conclusions

In this work, the crystal structure, microstructure, and electrical properties of (1-x)LSCN + xLCNZ (x = 0.0–1.0) composite ceramics were investigated by solid-state reaction experiments. With the addition of LCNZ, the impurity phases of NiO and $La_{1.2}Sr_{0.8}NiO_4$ appeared in the composite ceramics. The densification level deteriorated and electrical conductivity decreased as the proportion of LCNZ varied in x = 0.0–0.8. The TCR changed from positive to negative due to the contents of LCNZ and impurity phases increased. Zero TCR could be realized around $0.6 < x < 0.8$ and relatively low absolute TCR values could be achieved as the amount of LCNZ in the range of x = 0.4–0.8. And the ceramic of 0.6LSCN + 0.4LCNZ manifested the optimal performances: conductivity = 1923 S/cm, TCR = 379.54 ppm/℃, and relative density = 95.05%. Consequently, the composite ceramics of LSCN + LCNZ are potentially economical materials for the functional phase of thick film resistors.

Declarations

Acknowledgements

This work was supported by the Sichuan Science and Technology Major Projects (Grant No. 2019ZDZX0026), National Key Research and Development Project (Grant No. 2017YFB0406300), Natural Science Foundation of China (Grant No. 61841102, 61901142), and Sichuan Science and Technology Program (Grant Nos. 2019YFG0280).

References

[1] A. Shrivastava, A. Amin, B. Sood, M. Azarian, M. Pecht, M. Zagami, M. Frederick, Thick film resistor failures, Proceeding of the 34rd International Symposium for Testing and Failure Analysis, (2008) 197-205.

[2] D. Ortolino, J. Kita, K. Beart, R. Wurm, S. Kleinewig, A. Pletsch, R. Moos, Failure of electrical vias manufactured in thick-film technology when loaded with short high current pulses, Microelectron Reliab, 56 (2016) 121-128.

[3] N. White, Thick Films, in: S. Kasap, P. Capper (Eds.) Springer Handbook of Electronic and Photonic Materials, Springer International Publishing, Cham, (2017) 711-713.

[4] Y. Imanaka, Multilayered low temperature cofired ceramics (LTCC) technology, Springer Science & Business Media (2005), 83-100.

[5] M. Hrovat, Z. Samardžija, J. Holc, D. Belavič, The development of microstructural and electrical characteristics in some thick-film resistors during firing, J. Mater. Sci., 37 (2002) 2331-2339.

[6] M. Hrovat, J. Holc, M. Jakubowska, K. Kielbasinski, K. Makarovič, D. Belavič, Subsolidus phase equilibria in the CaO-poor part of the RuO_2–CaO–SiO_2 system, Mater. Res. Bull., 45 (2010) 2040-2043.

[7] C.-J. Ting, Interactions between Ruthenia-Based Resistors and Cordierite-Glass Substrates in Low-Temperature, J. Am. Ceram. Soc., 83 (2000) 2945-2954.

[8] M. Hrovat, Z. Samardzija, J. Holc, D. Belavic, Microstructural, XRD and electrical characterization of some thick film resistors, J. Mater. Sci. Mater. Electron., 11 (2000) 199-208.

[9] A. Alessandrini, G. Valdrè, B. Morten, M. Prudenziati, Electric force microscopy investigation of the microstructure of thick film resistors, J. Appl. Phys., 92 (2002) 4705-4711.

[10] A.W. Stadler, A. Kolek, Z. Zawiślak, K. Mleczko, M. Jakubowska, K.R. Kiełbasiński, A. Młożniak, Noise properties of Pb/Cd-free thick film resistors, J. Phys. D: Appl. Phys., 43 (2010) 265401.

[11] S. Achmatowicz, M. Jakubowska, E. Zwierkowska, M. Primovitch, Low Cost, Thick Film Resistive Compositions without the Use of Noble Metals, Microelectron. Int., 12 (1995) 23-25.

[12] A.D. Garje, R.C. Aiyer, Effect of firing temperature on electrical and gas-sensing properties of nano-SnO_2-based thick-film resistors, Int. J. Appl. Ceram. Technol, 4 (2007) 446-452.

[13] F. Zhang, G. Duan, L. Cao, D.a. Yang, Z. Liu, Preparation and properties of antioxidative BaO–B_2O_3–SiO_2 glass-coated Cu powder for copper conductive film on LTCC substrate, J. Mater. Sci. Mater. Electron., 29 (2018) 130-137.

[14] T. Rovensky, A. Pietrikova, I. Vehec, L. Livovsky, Stability of miniaturized non-trimmed thick- and thin-film resistors, Microelectron Reliab, 84 (2018) 88-94.

[15] P.T. Long, T. Manh, T. Ho, V. Dongquoc, P. Zhang, S. Yu, Magnetocaloric effect in $La_{1-x}Sr_xCoO_3$ undergoing a second-order phase transition, Ceram. Int., 44 (2018) 15542-15549.

[16] K. Iwasaki, T. Ito, T. Nagasaki, Y. Arita, M. Yoshino, T. Matsui, Thermoelectric properties of polycrystalline $La_{1-x}Sr_xCoO_3$, J. Solid State Chem., 181 (2008) 3145-3150.

[17] H. Kozuka, K. Ohbayashi, K. Koumoto, Electronic conduction in La-based perovskite-type oxides, Sci. Technol. Adv. Mater., 16 (2015) 026001.

[18] A. Chrzan, S. Ovtar, P. Jasinski, M. Chen, A. Hauch, High performance $LaNi_{1-x}Co_xO_{3-\delta}$ (x = 0.4 to 0.7) infiltrated oxygen electrodes for reversible solid oxide cells, J. Power Sources, 353 (2017) 67-76.

[19] V. Vulchev, L. Vassilev, S. Harizanova, M. Khristov, E. Zhecheva, R. Stoyanova, Improving of the thermoelectric efficiency of $LaCoO_3$ by double substitution with nickel and iron, J. Phys. Chem. C, 116 (2012) 13507-13515.

[20] P. Migiakis, J. Androulakis, J. Giapintzakis, Thermoelectric properties of $LaNi_{1-x}Co_xO_3$ solid solution, J. Appl. Phys., 94 (2003) 7616-7620.

[21] A. Mineshige, M. Inaba, T. Yao, Z. Ogumi, K. Kikuchi, M. Kawase, Crystal structure and metal–insulator transition of $La_{1-x}Sr_xCoO_3$, J. Solid State Chem., 121 (1996) 423-429.

[22] B. Liu, Y. Wang, G. Liu, H. Feng, H. Yang, J. Sun, Electrical transport properties of $La_{1-x}Sr_xCoO_3$ thin films, J. Appl. Phys., 120 (2016) 154103.

[23] H. Kozuka, K. Ohbayashi, K. Koumoto, $LaCo_{1-x}Ni_xO_3$ with Improved Electrical Conductivity, Inorg. Chem., 51 (2012) 9259-9264.

[24] V. Kumar, R. Kumar, D. Shukla, S. Gautam, K. Hwa Chae, R. Kumar, Electronic structure and electrical transport properties of $LaCo_{1-x}Ni_xO_3$ ($0 \leq x \leq 0.5$), J. Appl. Phys., 114 (2013) 073704.

[25] Y. Lu, Y. Li, D. Chen, R. Peng, Q. Yang, H. Su, Z. Tao, S. Zhang, Experimental and theoretical study on enhanced electrical properties of nickel-substituted $La_{0.5}Sr_{0.5}CoO_{3-\delta}$ ceramics, J. Eur. Ceram. Soc., 40 (2020) 3049-3056.

[26] J. Androulakis, J. Giapintzakis, Magnetoresistance in $LaNi_{1-x}Co_xO_3$ ($0.3 \leq x \leq 0.6$), Physica. B., 405 (2010) 107-112.

[27] Y. Lu, Y. Li, D. Chen, R. Peng, Q. Yang, H. Su, S. Zhang, The sintering and electrical properties of Zn-substituted $LaCo_{0.4}Ni_{0.6}O_3$ ceramics based upon experiments and calculations, Ceram. Int., (2020).

[28] I. Kagomiya, S. Matsumoto, K.-i. Kakimoto, H. Ohsato, H. Sakai, Y. Maeda, Controlling temperature coefficient of resistivity in $La_{1-x}Sr_xMnO_3$ ceramics, Mater. Lett., 63 (2009) 2452-2455.

[29] R. Peng, Y. Li, G. Yu, Y. Lu, S. Li, Effect of Co^{2+} Substitution on the Microwave Dielectric Properties of $LiZnPO_4$ Ceramics, J. Electron. Mater., 47 (2018) 7281-7287.

[30] J. Tang, R. Dass, A. Manthiram, Comparison of the crystal chemistry and electrical properties of $La_{2-x}A_xNiO_4$ (A = Ca, Sr, and Ba), Mater. Res. Bull., 35 (2000) 411-424.

[31] H. Chen, Y. Lu, W. Hwang, Characterization of sputtered NiO thin films, Surf. Coat. Technol., 198 (2005) 138-142.

[32] J. Ma, M. Theingi, Q. Chen, W. Wang, X. Liu, H. Zhang, Influence of synthesis methods and calcination temperature on electrical properties of $La_{1-x}Ca_xMnO_3$ (x=0.33 and 0.28) ceramics, Ceram. Int., 39 (2013) 7839-7843.

[33] D. Li, Q. Chen, Z. Li, Y. Li, H. Zhang, Y. Zhang, Effects of silver doping on structure and electrical properties of $La_{0.67}Ca_{0.23}K_{0.1}MnO_3$ polycrystalline ceramic, Ceram. Int., 44 (2018) 3448-3453.

[34] R. Peng, Y. Li, Y. Lu, Y. Yun, W. Du, Z. Tao, B. Liao, High-performance microwave dielectric composite ceramics sintered at low temperature without sintering-aids, J. Alloys Compd., 831 (2020) 154878.

Figures

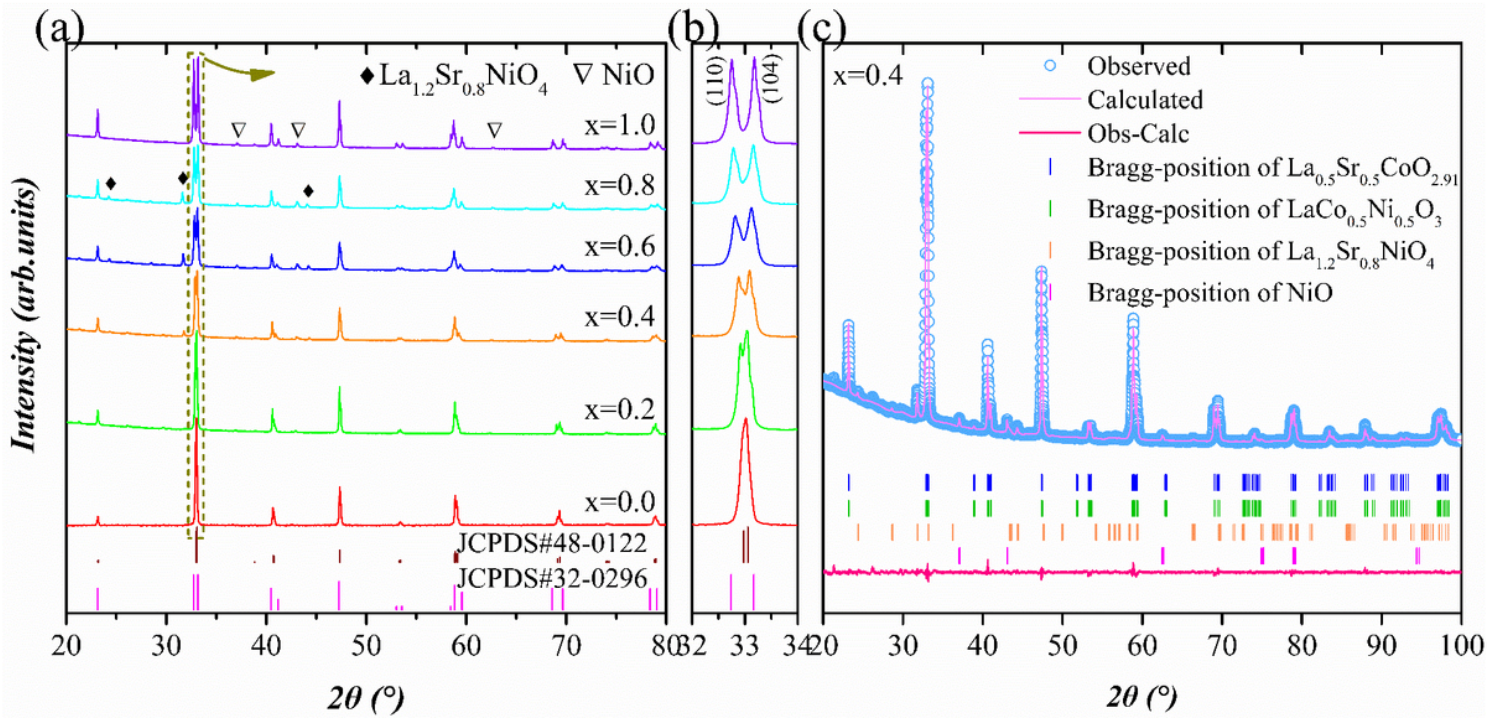

Figure 1

(a–b) XRD patterns of (1-x)LSCN + xLCNZ (x = 0.0–1.0) composite ceramics; (c) refined XRD pattern of 0.6LSCN + 0.4LCNZ ceramic.

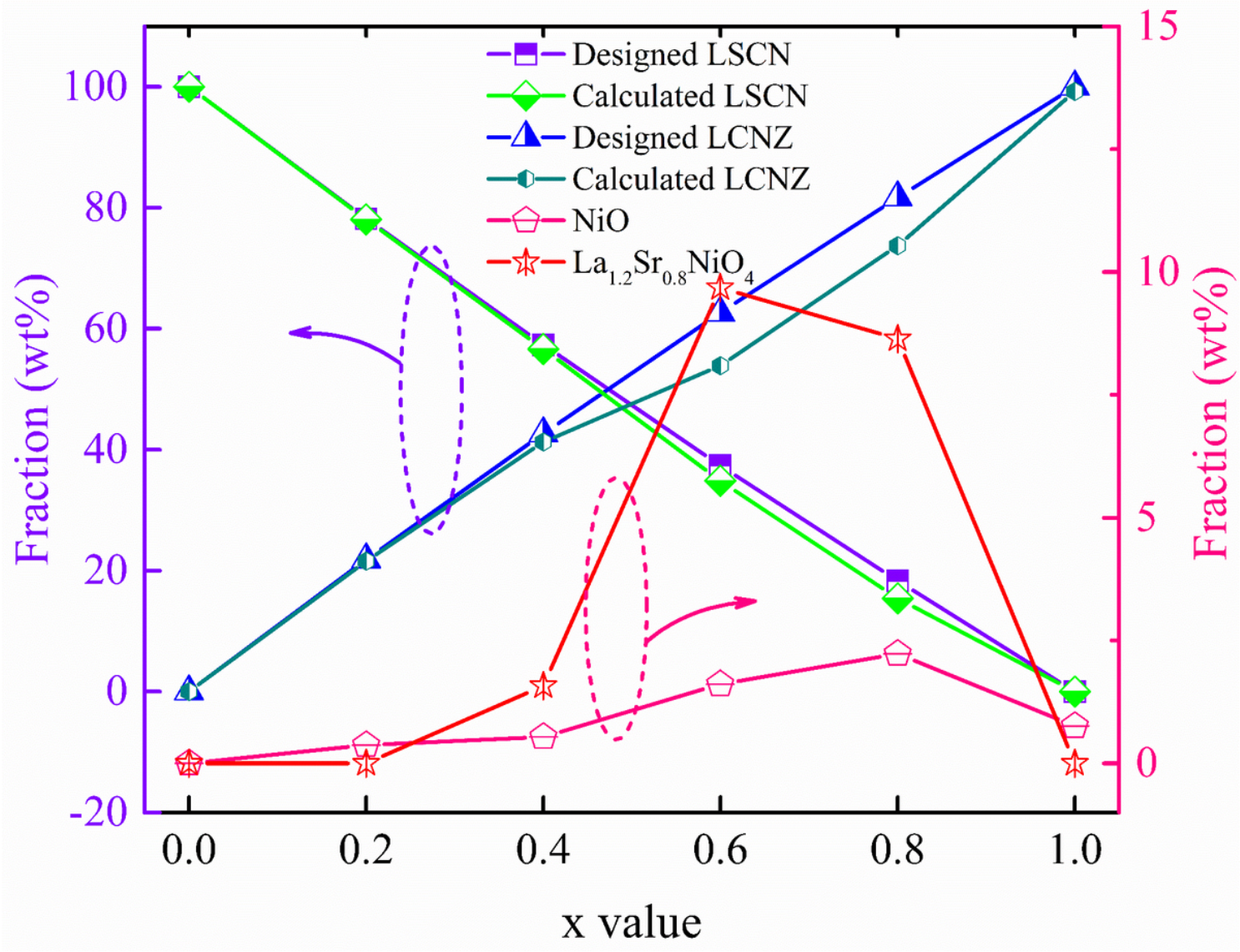

Figure 2

Designed and calculated fraction values of each phase in (1-x)LSCN + xLCNZ (x = 0.0–1.0) composite ceramics.

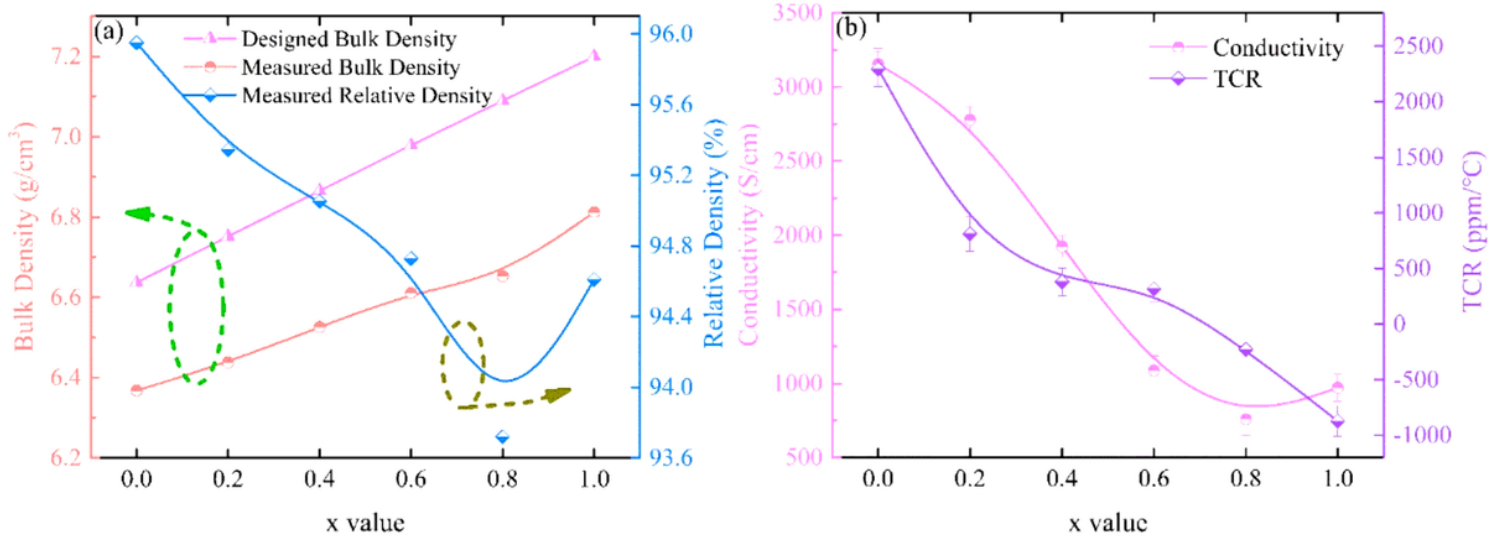

Figure 3

(a) Designed bulk density, measured bulk density and measured relative density, (b) conductivity and TCR of (1-x)LSCN + xLCNZ (x = 0.0–1.0) composite ceramics.

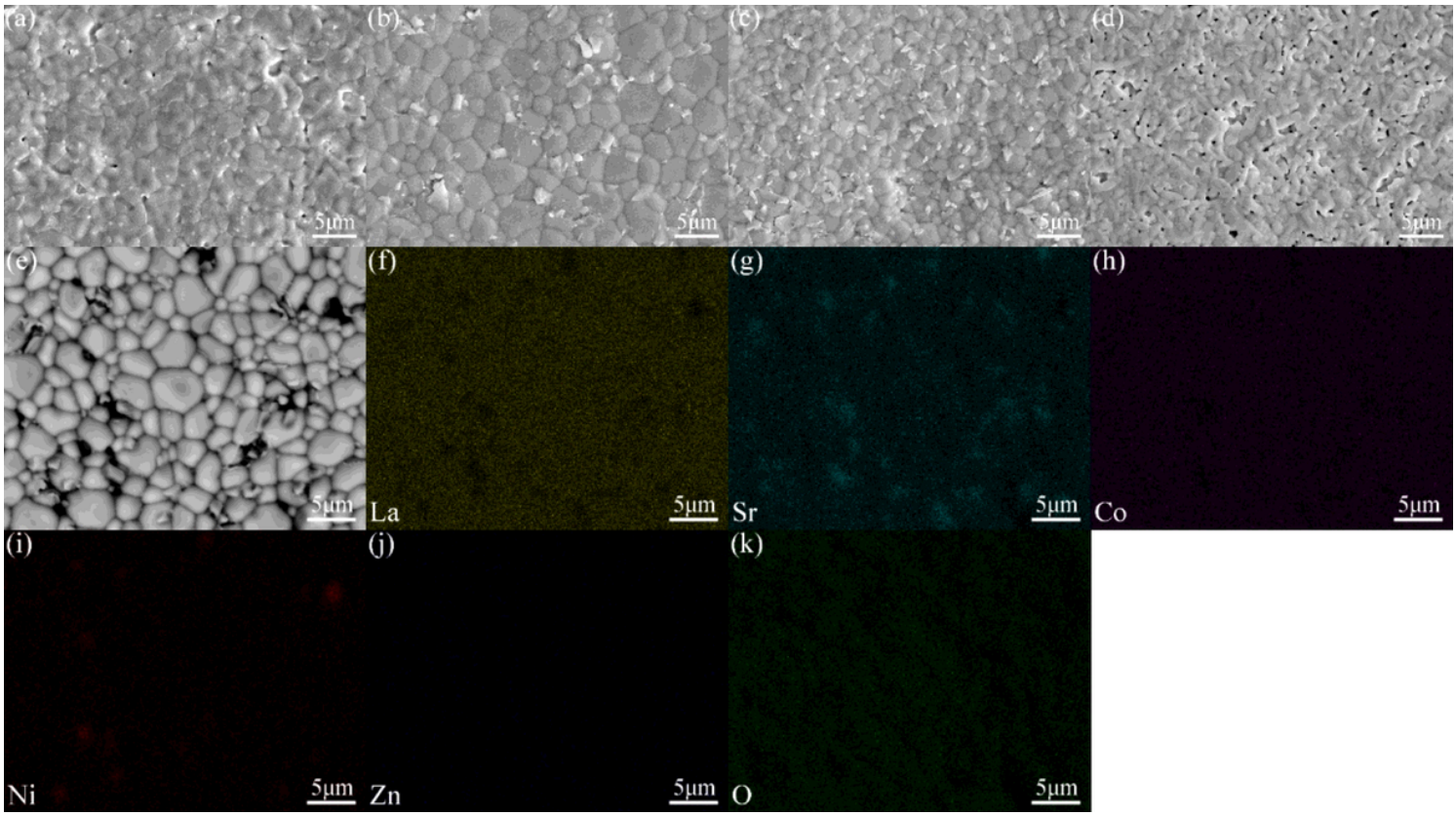

Figure 4

SEM images of (1-x)LSCN + xLCNZ (x = 0.2–0.8) composite ceramics: x=0.2 (a), x=0.4 (b), x= 0.6 (c), x=0.8 (d); EDS mapping images of 0.6LSCN + 0.4LCNZ ceramic (e–k).

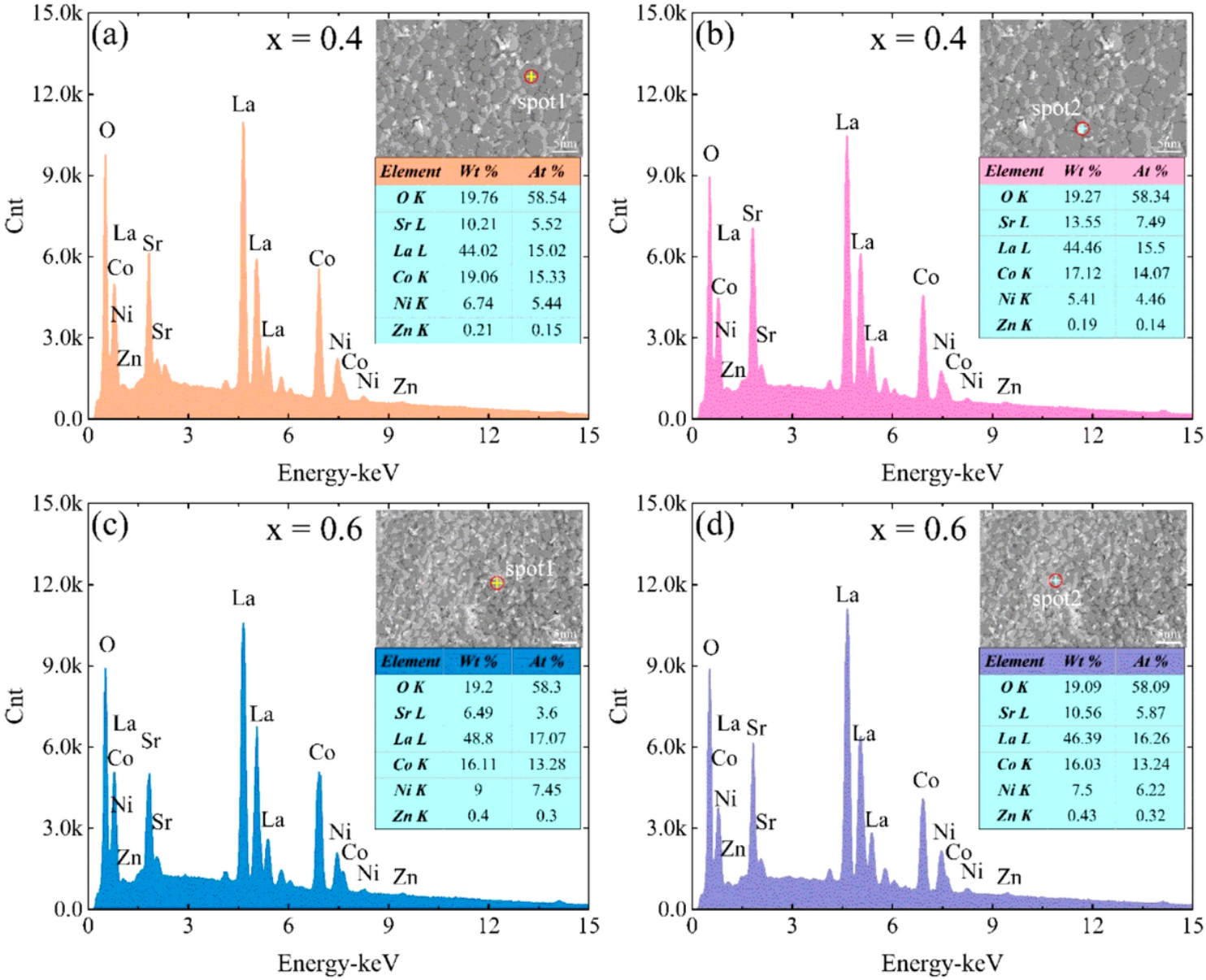

Figure 5

EDS results of (1-x)LSCN + xLCNZ (x = 0.4–0.6) composite ceramics: (a–b) x=0.2, (c–d) x=0.6.